Design and Preliminary Results from a High-Temperature SQUID Microscope for Nondestructive Evaluation

M. A. Espy, L. Atencio, A. Matlashov, and R. H. Kraus, Jr. (P-21)

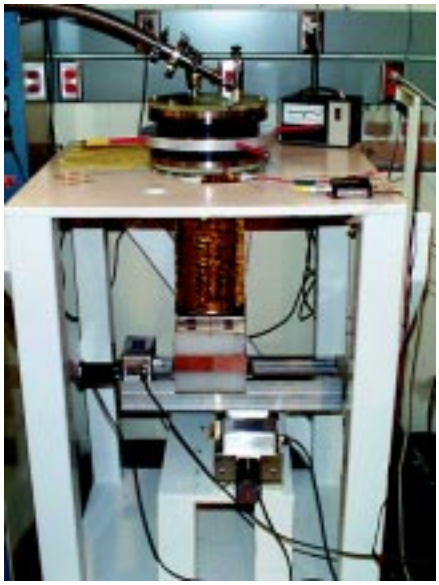

Fig. 1 Photograph of the SQUID microscope dewar operating in our laboratory.

The superconducting quantum interference device (SQUID) is the most sensitive detector of magnetic fields known. SQUIDs are so sensitive that they are able to detect magnetic fields ten billion times smaller than Earth's. Because of their incredible sensitivity, SQUIDs can be used to detect the minute magnetic fields associated with biological function, such as the magnetic fields present outside the head due to neuronal activity in the brain. The primary objective of our work has been developing biological applications for SQUID measurements, such as magnetic mapping of brain function. In addition, we have applied SQUID sensor measurement and analytic approaches to the problem of nondestructive evaluation of stockpile weapons components as part of Los Alamos National Laboratory's Enhanced Surveillance Program, a component of the Department of Energy's (DOE's) science-based stockpile stewardship (SBSS) program.

We have designed a SQUID "microscope" that uses a liquid-nitrogen-cooled SQUID sensor to map magnetic fields induced in a sample (Fig. 1). Similar instruments are described by Black[1]; Kirtley, *et al.*[2]; and Cochran, *et al.*[3]. Our microscope characterizes the features of interest in the sample (*e.g.*, defects due to aging) by detecting anomalies in the induced magnetic field. To address the needs of SBSS, we designed an instrument that is sensitive to small features buried under several intervening layers (~1–20 mm) of conducting and/or nonconducting materials, and that is robust enough to operate even in magnetically noisy, unshielded environments. Our microscope, which has been operational since September 1997, has primarily been applied to specific nondestructive evaluation problems such as detecting and determining the width of buried "seams" inside nuclear components without having to take the components apart. This research highlight describes how the microscope works, and it presents the results of several tests that demonstrate the usefulness of this technology.

Compared with other technologies, SQUIDs are well suited to many problems of buried features such as cracks, pits, or other structural abnormalities. A technique such as complex impedance measurement has to go to lower drive frequencies, ω, to get the required skin depth, δ (the distance that the eddy currents penetrate into the material before falling to ~37% of their magnitude at the surface). As shown in the equations below, the lower the frequency the greater the skin depth (and the more deeply one can probe for a defect). However, lower frequencies also result in a corresponding decrease in signal strength, V, as shown:

$$\delta = \sqrt{\frac{2\rho}{\omega\mu_0}} \quad and \quad V \propto \omega,$$

where ρ is the resisitivity of the material. Ultrasound, on the other hand, has difficulties with signal reflection at the boundaries of material layers that are sonic absorbers (most plastics and electrical insulators), reducing the sensitivity to features below such layers. Finally, radiographic techniques can be expensive, nonportable, and insensitive to small one-dimensional features. SQUIDs are not limited by these shortcomings. SQUID sensitivity does not depend on frequency, enabling these sensors to be used for detecting features and defects over

a broad range of material depths. The induction signal at a given frequency depends only on ρ, not on gaps or intervening layers. Also, a SQUID system can be portable and relatively inexpensive.

Figure 2 is a schematic diagram of the SQUID microscope and the data acquisition system. The main component of the microscope is the dewar, which is shown mounted in a wooden stand in Fig. 1. The inner chamber of the dewar is filled with liquid nitrogen. The high-temperature superconducting SQUID, a bare Conductus "Mr. SQUID"™ chip with an area of 30 × 30 μm and a sensitivity of 700 nT/Φ_0, is located in vacuum on the tip of a sapphire cold-finger, which is in contact with the liquid nitrogen reservoir. A 1-cm-diameter, 0.25-mm-thin quartz window is mounted on the bottom of the dewar immediately below the SQUID. During operation, the SQUID is located ~0.13 mm from the window. The cold-finger keeps the SQUID at ~78°K despite its proximity to the outside world (~300°K). The small area of the SQUID allows the instrument to operate without shielding in the magnetically noisy environment of our laboratory. Eventually, a second SQUID will be installed at the base of the sapphire cold-finger to construct a first-order gradiometer.[4,5]

The eddy-current induction coils, used to induce a magnetic field in the sample, are located on the outside of the dewar just beneath the window. The induction coils were designed to produce a "null" in the magnetic field at the location of the SQUID, thus using little or no sensor dynamic range for the induction signal. Two designs have been used thus far. The first consisted of two pairs of "double-D" coils rotated by 90°. In this design, the large size of the double-D coils relative to the sample sizes produced asymmetric eddy-currents at the sample edges resulting in large anomalous signals. We were able to avoid most of these edge effects by using the second design, a circle-within-rectangle coil, which is shown in Fig. 2. Two adjustable current generators with 150-mA maximum output current, driven by a common function generator, provide current to the two induction coils. The function generator also provides a reference signal to the lock-in amplifier.

Prior to data acquisition, the sample is centered on the two-axis scanning stage located below the dewar. The distance between the SQUID and the top of the sample is typically 1 mm. The current in the induction coils is adjusted until the SQUID measures a minimum magnetic field. During data acquisition, a personal computer controls the SQUID electronics (Conductus pcSQUID™ electronics) and the motion control system. Low-magnetic-noise stepper motors move the sample, and the SQUID electronics provide the SQUID's response amplitude and phase to the lock-in amplifier. At each point, the personal computer reads the lock-in amplifier, which provides data based on the amplitude and phase of the SQUID responses relative to the reference signal.

Initial data were taken using 150- × 150- × 1.5-mm-thick aluminum plates. Blank plates (unperturbed rolled-stock) and flawed plates (with induced cracks and holes) were examined both individually and

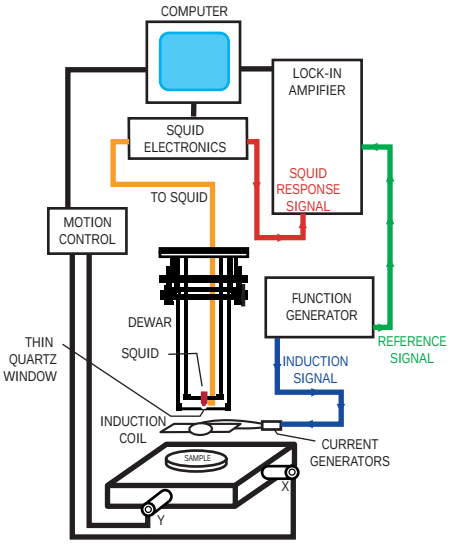

Fig. 2 Schematic drawing of the SQUID microscope and data acquisition system.

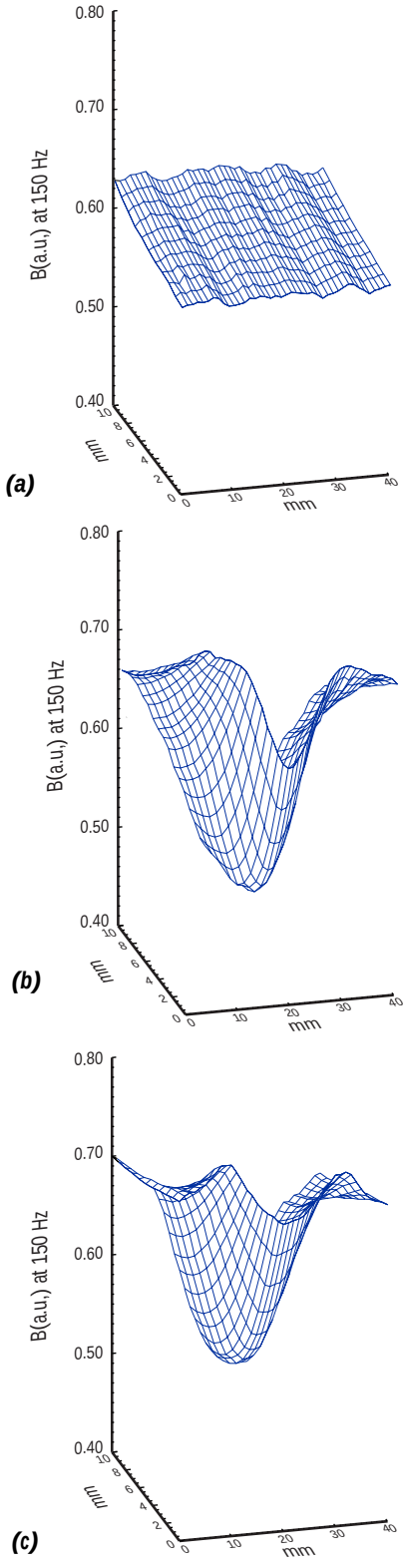

Fig. 3 Scan of a blank aluminum plate (a), cracked aluminum plate (b), and cracked aluminum plate covered by an unflawed plate (c). Induction frequency was 150 Hz.

stacked. Figure 3 plots the raw amplitude from the lock-in amplifier as a function of position for an unflawed aluminum plate (a), a plate with a crack (b), and a plate with a crack all the way through the 1.5-mm plate material covered by an unflawed plate (c). The presence of the crack is indicated by a valley in which the width of the valley is proportional to the width of the crack. Figure 4 presents raw data for an aluminum plate with holes of various diameters. The presence of a hole is indicated by a two-lobed signal in which the spacing between the lobes is proportional to the diameter of the hole. (The spikes in the data occur where the SQUID electronics momentarily unlocked.) Even 1-mm-diameter holes are visible. Data were also collected for this same plate covered by an unflawed plate (not shown), and all of the holes were still visible (background subtraction was applied to resolve the smallest two holes).

Following these initial data, we analyzed a titanium-tungsten sample that had a stress fracture. A photograph of this sample is shown in Fig. 5a. The results of a single-pass scan lengthwise over the sample are shown in Figure 5b. This sample was slightly ferromagnetic, which poses a challenge to an instrument as sensitive as a SQUID. Simply moving a slightly magnetic object beneath a SQUID can be enough to overwhelm the instrument. However, because of the small SQUID pick-up coil on this device, we were still able to make the scan. This suggests that the instrument should be flexible enough to handle "real-world" objects that might also be slightly magnetized. The stress fracture was clearly observed, demonstrating sensitivity to severe lattice defects that do not necessarily evidence a physical separation. This data set illustrates that while the instrument can localize defects on the submillimeter scale, it is sensitive to defects that are orders of magnitude smaller. It is also interesting to note that the chamfer at the left edge of the sample shown in Fig. 5a is visible in the scan at 633 Hz.

To further test the capabilities of our microscope, we analyzed flaws in fiberglass plates coated with 100 μm of copper. For one of these plates, we carved the initials "P-21" through the copper to expose the fiberglass beneath. This sample is shown in Fig. 6a. Figure 6b shows the raw data from a scan of this plate. The letters are clearly visible.

In another set of these plates (not shown), we carved closely spaced pairs of scratches. The scratches were ~100-μm wide, 75-mm long, and penetrated the 100-μm copper layer. The scratch pairs were separated by different distances. The scratches that were 5 mm apart were resolved. The scratch-pairs that were 3-mm and 1-mm apart each appeared as one scratch, although the 3-mm scratch-pair was wider. These data indicate the need to design induction coils tailored to the specific type of defect being sought. Improved induction coil design and the use of a SQUID array will ultimately provide the highest resolution.

To specifically address the SBSS problem of quantitatively monitoring the evolution of known seams in nuclear components over time, we designed a simple test sample using two 150- × 150- × 10-mm-thick titanium plates. Titanium was chosen because it has conductivity similar to the specific materials of interest.

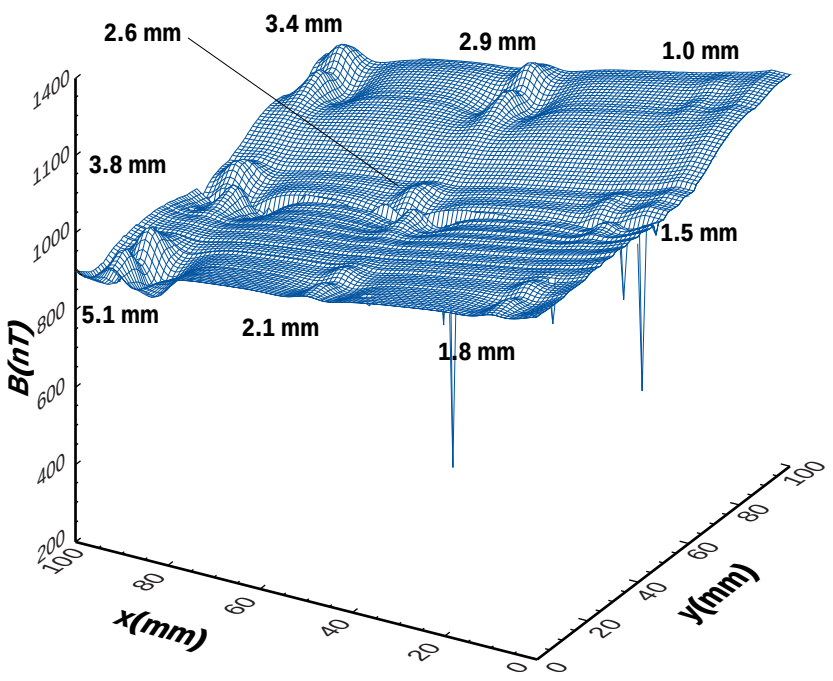

Fig. 4 Raw data for aluminum plate with holes of various diameters. Induction frequency was ~300 Hz.

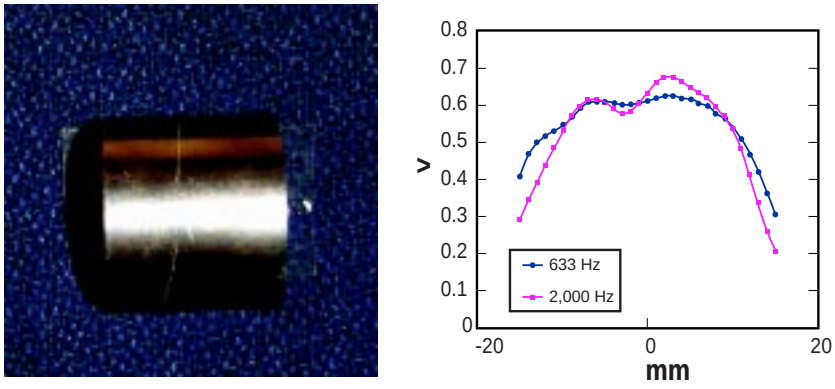

(a) *(b)*

Fig. 5 (a) Photograph of titanium-tungsten surrogate with a stress fracture. (b) Data from a single scan lengthwise down the surrogate.

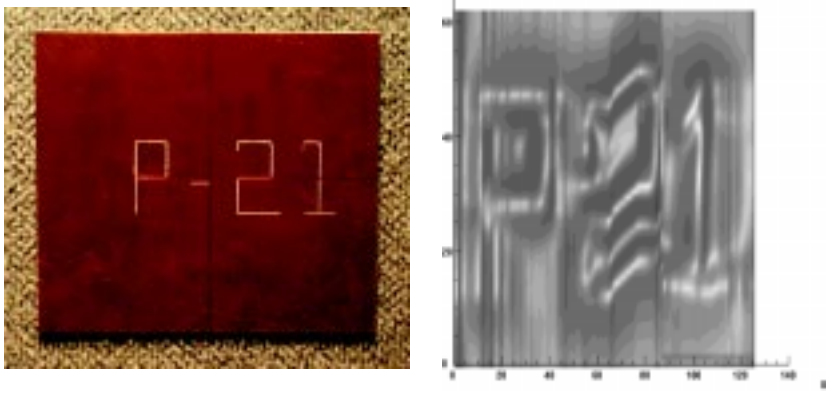

(a) *(b)*

Fig. 6 (a) Photograph of 150- × 150-mm copper-plated fiberglass plate with "P-21" scratched into the 100-μm-thick copper layer. (b) Raw data from a scan of this plate.

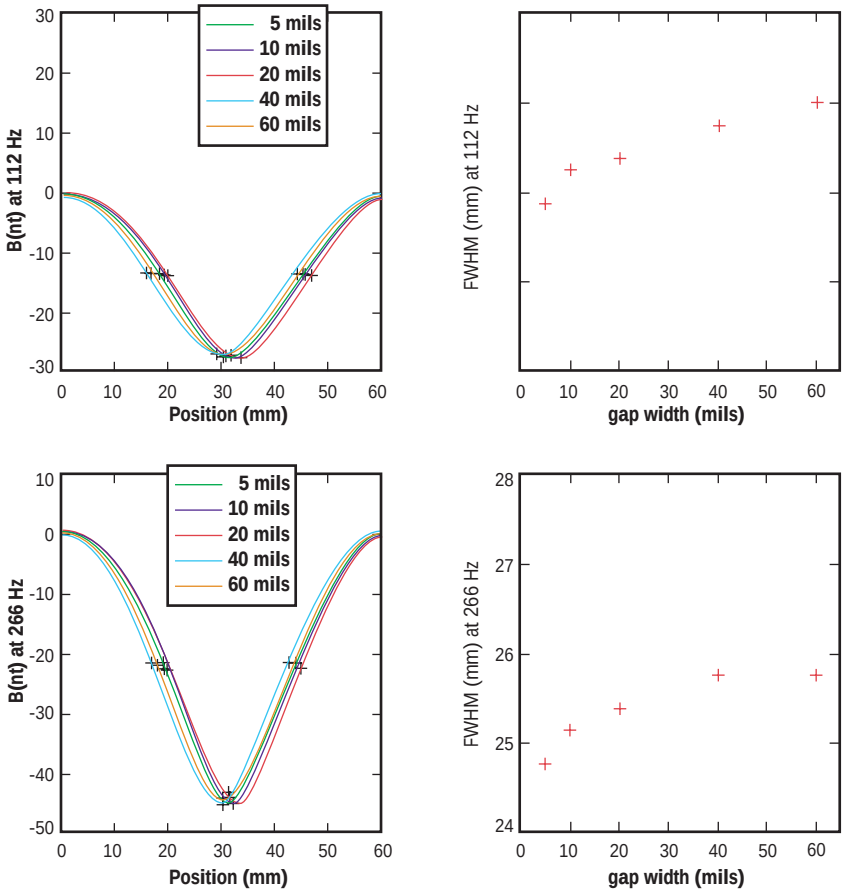

Fig. 7 Data for seams of various widths in a titanium plate at 112 Hz and 266 Hz. The seams were buried under 1 cm of unflawed plate.

A seam was simulated by cutting one of the plates in half and inserting spacers. In real SBSS cases, seams are typically buried under ~1 cm of conducting material, making it very challenging to determine whether they are changing width as they age. To simulate such a case, the second unflawed titanium plate was stacked on top of the "seamed" plate.

Our goal was to obtain quantitative information about the width of the buried seam. Scans were taken for seam widths of 5, 10, 20, 40, and 60 mils at 112-Hz and 266-Hz induction frequencies. Results are presented in Fig. 7. The response to the seam appears as a valley in the data. The full-width-at-half-minimum (FWHM), or the width of the valley when its height is at half its minimum value, was fit for each scan and is plotted as a function of seam width. As expected, the amplitude of the response grows with frequency. The lower frequency (112 Hz) appears to show the trend of FWHM versus seam width most clearly. This is also somewhat expected; at 112 Hz the skin depth is 2.2 cm (recall that the seam is 1 cm beneath a titanium plate) while the skin depth for 266 Hz is 1.4 cm. Another interesting feature of the data is that at both 112 Hz and 266 Hz the curve of FWHM as a function of seam width appears to be leveling off. One possible explanation is that the response should fall off as the seam width increases beyond the "field of view" of the SQUID.

We have begun modeling the titanium seam width problem using OPERA, a commercial electromagnetic finite-element code developed by Vector Fields, Inc. We anticipate that the results of this modeling effort will enable us to design new induction coils sensitive to specific features of interest at particular depths in a sample. In addition, we have fabricated a series of copper calibration plates with 75-mm-long scratches of depths and widths ranging from 0.125 to 1 mm. We intend to use data taken with these plates in conjunction with the model to further quantify the resolution of the instrument and the competing effects of depth and width of buried seams.

We are also pursuing a number of other improvements to our technique. In collaboration with Oak Ridge National Laboratory, a five-axis motion control system with low magnetic noise is being developed that will enable us to examine spherical and cylindrical samples. In addition, collaborators at Allied Signal/Kansas City Plant are currently developing flux-locked loop electronics with high slew-rate to improve operations in electromagnetically noisy environments. We are also designing a SQUID-array to enhance the resolution of the instrument. While our results are already promising, these improvements will ensure that the SQUID microscope offers useful, accurate results for SBSS and other applications.

References

[1] R. C. Black, "Magnetic Microscopy using a Superconducting Quantum Interference Device," Ph.D. thesis, University of Maryland (1995).

[2] J. R. Kirtley, M. B. Ketchen, C. C. Tsuei, J. Z. Sun, W. J. Gallagher, L. S. Yujahnes, A. Gupta, K. G. Stawiasz, and S. J. Wind, "Design and Applications of a Scanning SQUID Microscope," *IBM Journal of Research and Development* **39**, 655 (1995).

[3] A. Cochran, J. Kuznik, C. Carr, L. N. C. Morgan, and G. B. Donaldson, "Experimental Results in Nondestructive Evaluation with High Temperature Superconducting SQUIDs," *Institute of Physics Conference Series* **148**, 1511 (1995).

[4] M. A. Espy, R. H. Kraus, Jr., E. R. Flynn, and A. Matlashov, "Two Methods for a First Order Hardware Gradiometer using Two High Temperature Superconducting Quantum Interference Devices," *Review of Scientific Instruments* **69**, 123 (1998).

[5] Y. Tavrin, H. J. Krause, W. Wolf, V. Glyantsev, J. Schubert, W. Zander, A. Haller, and H. Bousack, "Eddy-Current Technique with High Temperature Superconducting SQUID Gradiometer for Nondestructive Evaluation of Nonmagnetic Metallic Structures," *Institute of Physics Conference Series* **148**, 1519 (1995).